



# Design of dermal electrospun replacement

ANTE AGIĆ<sup>1</sup>  
MILORAD NIKITVIĆ<sup>2</sup>  
BUDIMIR MIJOVIĆ<sup>3</sup>

<sup>1</sup>Faculty of Chemical Engineering  
and Technology  
University of Zagreb  
Marulićev trg 19  
10000 Zagreb, Croatia

<sup>2</sup>College for Information Technologies  
10000 Zagreb, Croatia

<sup>3</sup>Faculty of Textile Technology  
University of Zagreb  
Prilaz b. Filipovića 28a  
10000 Zagreb, Croatia

**Correspondence:**

Ante Agić  
Faculty of Chemical Engineering  
and Technology  
University of Zagreb  
Marulićev trg 19  
10000 Zagreb, Croatia  
E-mail: aagic@fkit.hr

**Key words:** electrospinning, dermal  
scaffold, multiscale design

## Abstract

**Background and Purpose:** This study is related to the design of advanced dermal scaffolds (non-woven fibrous mats) to provide multifunctional properties.

**Materials and Methods:** The nanofibre fabric from poly ( $\epsilon$ -caprolactone) (PCL) solutions in acetone were produced by electrospinning. Based on SEM and its stochastic fibre characterization, equivalent fabric was generated by computer. Fibres network was created by random deposition of elastic straight segments within a representative volume element (RVE). Elastic and permeability properties determined experimentally and numerically.

**Results:** The fibres diameter produced fibrous structure depends on solution concentration and electric field, what have been identified by surface response methodology. Effective Young's modules for fibrous network measured and predicted by numerical model depend on fibres density and fibres diameter. Calculated data for permeability and pore distribution were compared with models for fibrous media with acceptable error level.

**Conclusions:** Effective elastic and permeability properties are determined by separate computational models. The scaffold multiscale behaviour is commented with multiphysic design procedure.

## INTRODUCTION

Human skin is the largest organ which protects the body from disease and physical damage. It is composed of two major layers, the epidermis and the dermis (Figure 1). When the skin has been seriously damaged through disease or burns, the body cannot act fast enough to produce necessary replacement cells. For example, burn victims die from infection and loss of plasma. Skin grafts were developed as a way to prevent such consequences. Artificial skin grafts can be made in large quantities and be frozen for storage and shipping, making them available at any time. The artificial skin does not contain immunogenic cells, it is not rejected by the body, and finally it involves reduced rehabilitation time.

This research focuses on the creation of advanced dermal scaffolds (non-woven fibrous mats) to provide a functional three dimensional substrate, with enhanced properties. The purpose of tissue engineering is to regenerate biological tissues by the use of porous, degradable biomaterials (scaffolds) to deliver cells, genes, and/or proteins ('biologics'). The scaffold will provide temporary mechanical support and define tissue shape while delivering 'biologics' from internal pores and through release after degradation. The two primary requirements for a scaffold are temporary mechanical support and tissue regeneration

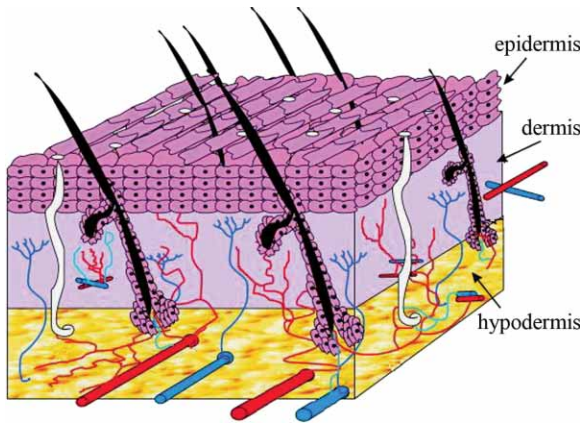


**Figure 1.** Human skin: cross-section.

through biologic delivery (1). Mechanical support can be defined through constitutive parameters poroelasticity continua. Tissue regeneration is related to mass transport characteristics like permeability, but depends also on cell material interaction parameters. Defined target properties are attained by distributing specified base materials at multiple length scales ranging from several nanometers to millimeters. Material distribution at the multiple material scale range («scaffold microstructure») has not been topic in structural design, but it is realized by fabrication processes. It is desirable to calculate effective scaffold properties like stiffness and permeability based on scaffold microstructure, so that the effect of these properties on tissue regeneration may better be predicted. Design is further complicated by the fact that target properties for mechanical support are opposed to those associated with enhanced tissue regeneration, essentially mass transport properties. Therefore, the best possible combination of mechanical support and mass transport relies on optimizing material distribution within a porous microstructure (2). The goal was to determine bounds of single effective properties (elasticity, conductivity, permeability) that can be attained at a specified porosity and how these materials should be arranged in three dimensional space. These bounds define what properties may theoretically be attained for a given base scaffold material. Numerous top-down and bottom-up nanofabrication technologies (such as electrospinning, chemical vapor deposition, self-assembly processes) are available to synthesize nanomaterials with fine microstructure (3). After decreasing material size into the nanoscale specific surface area, dramatically increased, surface roughness leads to superior physiochemical properties (i.e., mechanical, electrical, catalytic properties, etc.). Studies have demonstrated that nanostructured materials with cell favorable surface properties may promote greater amounts of specific protein interactions to more efficiently stimulate new tissue growth compared to conventional materials; this may be one of the main mechanisms why nanomaterials are superior to conventional materials. Tissue scaffolds were developed through electrospinning process which creates a non-woven fibrous construct of high

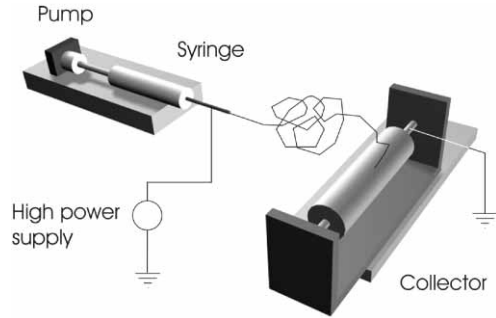


**Figure 2.** Electrospinning process.

permeability and proper mechanical integrity similar to the scale of the extracellular matrix of cells. Electrospinning is a fascinating processing technique capable of converting polymers into interconnected flexible nanofibrous structures, and it is particularly appealing for fabricating large sheets of scaffolds suitable for dermal implantation. When electric field increases beyond a critical value – at which repulsive electrical forces overcome the surface tension of polymer solution (or melt) droplet at the tip of the nozzle – a charged jet is ejected (Figure 2). As the jet travels to the collector, it either cools down (in case of the melt) or the solvent evaporates (in case of the solution) to produce ultrafine fibers in the form of a non-woven nanofabric.

The non-woven fabrics of electrospun fibers have unique properties, such as dramatically increased specific surface, excellent mechanical strength, and highly open porous structures. A number of nanofiber assemblies have been developed through electrospinning by incorporating functional agents to achieve antibacterial, magnetic properties. The morphology of electrospun fibers depends on a number of factors, such as solution properties (e.g., concentration, viscosity, conductivity, surface tension, etc.), processing conditions (e.g., electrical potential, collection distance, etc.), and ambient conditions (e.g., temperature, humidity, etc.). The goal of this paper was to examine the range of elastic and permeability properties that can be spanned using electrospinning approaches. These architectures can then be tested both *in vitro* to determine how well fabricated scaffold microstructures can match the computational design, and *in vivo* to determine if these designs will affect tissue regeneration (4).

## METHODS

### Elastic properties

Based on SEM and its stochastic fibre characterization, equivalent fabric was generated by computer. Fiber network was created by random deposition of elastic straight segments within a representative volume element (RVE). Nucleation sites were generated randomly inside a RVE and gave rise to the segment along randomly chosen directions. The line between two cross-links associated with the same segment defines fibred

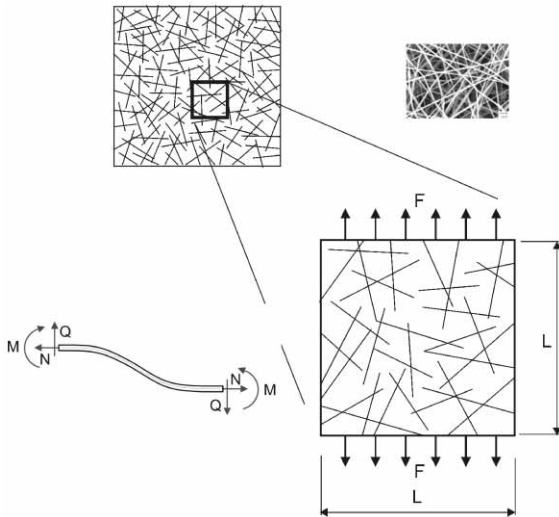


Figure 3. The finite element model of fiber net.

structural units (beam or truss element). Selecting directional vectors from probability distribution function allows generation of networks with equivalent structures as experimental SEM image. Effective mechanical properties of nanofiber sheets at the macro scale level can be determined using the two dimensional (2D) Timoshenko beam-network. The non-load bearing fiber segments were removed and trimmed to keep dimensions  $L \times L$  of the representative window (Figure 3). A line representative network model was replaced by finite element beam mesh. The number of intersections/unit area, probability distribution function and mean lengths were obtained from image analysis of electrospun sheets. We considered here tensile stress, and fibers were rigidly bonded to each other at every fiber-fiber crossing points. The problem was reduced to solution of the linear system of equations

$$[K] \cdot \{u\} = \{f\} \tag{1}$$

where  $\{u\}$  is global displacement vector,  $\{f\}$  global nodal force vector, and  $[K]$  global stiffness matrix (5). Effective

elasticity tensor can be determined by homogenization procedure by the following formula

$$\langle C_{ijkl} \rangle = \frac{1}{V_{RVE}} \int C_{ijkl}(x,y,z) dV \tag{2}$$

$$C_{ijkl}(x,y,z) = \frac{\partial U}{\partial \epsilon_{ij} \partial \epsilon_{kl}}$$

where  $U$  elastic deformation energy and  $\epsilon_{ij}$  deformation tensor, respectively.

### Pore network model

Many fibers form a 3D network of pore bodies and pore throats that constitute the microstructure of scaffold. In order to calculate permeability of the generated fiber network we need to construct the pore space of a scaffold by a network in which the bonds and sites represent pore throats and pore bodies, respectively. A grid was then imposed on images that closely mimics the topology of pore space, so that the lines that connect the grid points run more or less along pore throats, with the grid points being in pore bodies. Pore throats are channels that are formed between fibers. Pore bodies are the cavities where pore throats meet each other. Local coordination numbers, connectivity and their statistical distributions, are determined from pore network mesh. Each throat is characterized by effective radius and length, both of which follow, in general, some statistical distributions. Since we represent each pore throat effectively as a cylindrical pore of radius  $r_{ij}$  and length  $l_{ij}$ , the volumetric flow rate  $q_{ij}$  through the tube from the  $i$ -th to the  $j$ -th node is given by (Figure 4)

$$q_{ij} = \frac{\pi r_{ij}^4 \Delta p_{ij}}{8 \mu l_{ij}} \tag{3}$$

where  $\Delta p_{ij}$  is the pressure drop along the throat,  $\mu$  is effective viscosity, and  $l_{ij}$  is the throat's length.

The fluids are assumed incompressible, leading to conservation of volume flux at each node

$$\sum_{\{j\}} g_{ij} = 0 \tag{4}$$

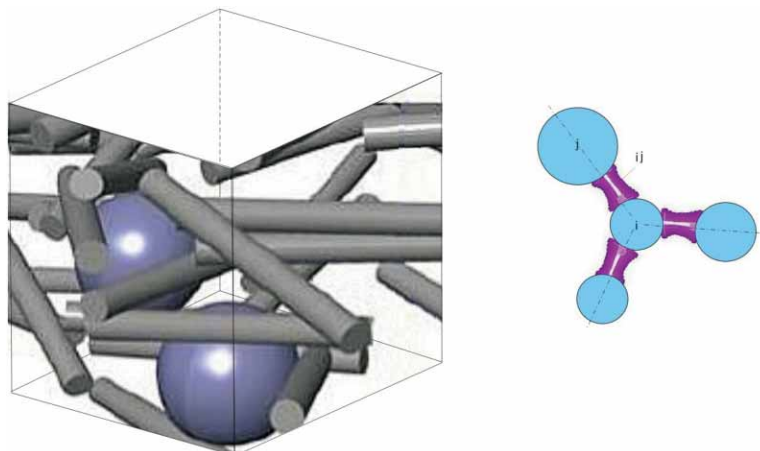


Figure 4. Pore net model.

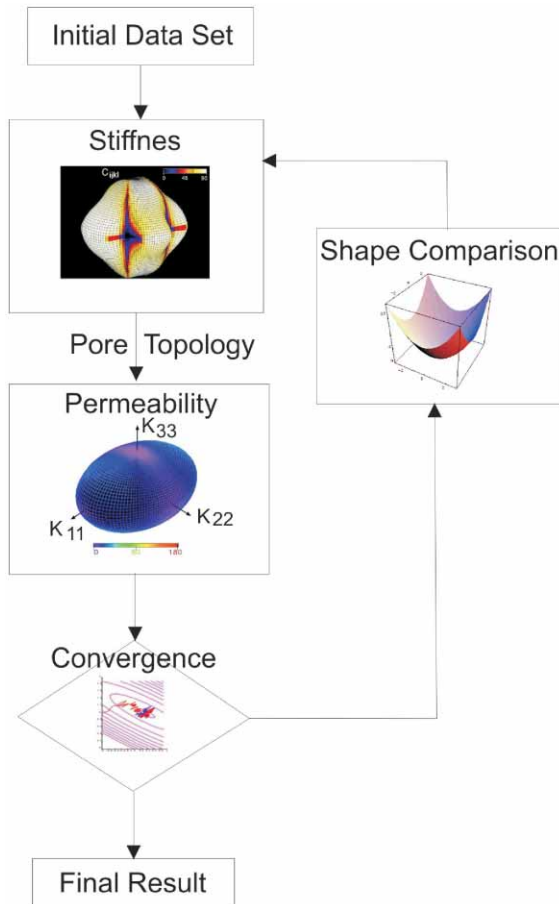


Figure 5. The multiphysics optimization scheme.

where  $q_{ij}$  is the volumetric flow rate through a tube connecting pore  $i$  and  $j$ . The sum is over all throats  $ij$  that are connected to pore body  $i$ . If we write equation (3) for every interior node  $i$  of the network, then together with equation (4) we obtain a set of simultaneous linear equations for nodal pressures. Subject to specified boundary conditions, we get matrix equation

$$[D] \cdot \{p\} = \{IT\} \tag{5}$$

where  $D$  is conductance matrix,  $\{p\}$  is pressure vector (internal nodes) and  $\{IT\}$  pressure vector on boundaries. The result of solution equation (5) is pressure distribution in the network. Assuming that the flow of a fluid in a fiber network is slow enough that the Darcy's law is applicable, then the flow properties of an anisotropic network are characterized by a symmetric and second rank permeability tensor  $K_{ij}$ , defined by

$$\langle v \rangle = -\frac{K_{ij}}{\mu} \nabla p \quad i, j = 1, 2, 3 \tag{6}$$

where  $\langle v \rangle$  is the average fluid velocity vector,  $\mu$  is the viscosity of the fluid, and  $\nabla p$  is the pressure gradient imposed on the porous medium. To compute the effective permeability of a fabric in given direction, a pressure gradient is imposed on the network along that direction.

### OPTIMAL DESIGN

The real issue for creating dermal scaffolds is to derive a microstructure design that will give the desired multi-functional properties. Inverse topology optimization method iteratively constructed the microstructure that provides the desired properties. Based on our previous study (6), we proposed multiphysics designing approach in which the first invariant of permeability tensor is maximized as objective function  $J$ , with constraints on desired effective elasticity tensors, and on porosity topology. Microstructure design for this problem, with the formal optimization statement has the following form

$$\begin{aligned} & \max J (K_{ii}^{scaffold}) \\ & \rho \\ & \text{subject to } \|C_{ijkl}^{scaffold}\| \leq \|C_{ijkl}^{target}\| \\ & 1 - \rho \leq \text{porosity} \end{aligned} \tag{7}$$

$$\rho = V/V_{RVE}$$

$C_{ijkl}^{target}$  is the target value of where effective elasticity tensor, and  $V_{RVE}$  and  $V$  denote representative volume element and volume of the solid material, respectively. Homogenization theory is used within an iterative optimization scheme to compute effective properties as part of objective function. Design approach creates a volumetric 3D design by replicating representative unit cells periodically in 3D space. Multiphysical optimization concept is schematically presented in Figure 5.

### EXPERIMENTAL PART OF THE STUDY

Poly( $\epsilon$ -caprolactone) (PCL) solutions (Sigma–Aldrich, mol. weight = 65,000) in acetone were produced by stirring the solvent and particulate polymer at 50 °C until the solid was fully dissolved. Electrospun PCL fibers were produced using a 20 ml/h solution flow rate, a 10–20 kV potential between the needle tip and 10–20 cm collector distance. Samples were collected at room temperature and certain humidity (30% RH). After deposition, the samples were exposed to a vacuum at room temperature for 8 h to ensure that residual solvent levels were not significant. Characterization of the tissue scaffolds included image analysis, tensile tests, and porosimetry measurements to demonstrate enhanced properties and preferred morphologies.

### RESULTS

Experimental data for fiber diameter produced fibrous structure depending on solution concentration and electric field have been identified. Based on surface response methodology (7) the coefficient  $A_{ij}$  in second-order model (eq. 8) was determined by multiple regression analysis using experimental data for electrospinning PCL solution.

Fiber diameter  $D$  is given by

$$D = A_{00} + A_{01}x + A_{10}y + A_{02}x^2 + A_{20}y^2 + A_{11}xy \tag{8}$$

where  $x$  and  $y$  PCL concentration and electric field, respectively.

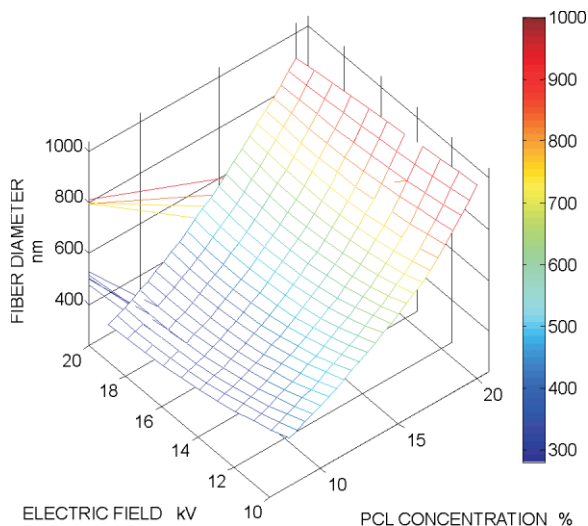


Figure 6. Fiber diameter dependence on solution concentration and electric field.

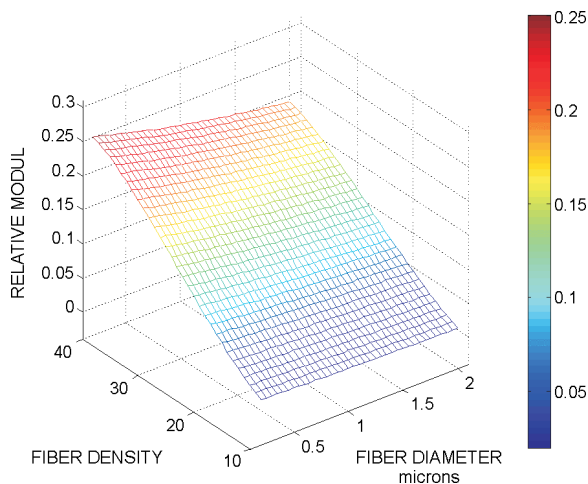


Figure 7. Modulus dependence on fiber density and diameter.

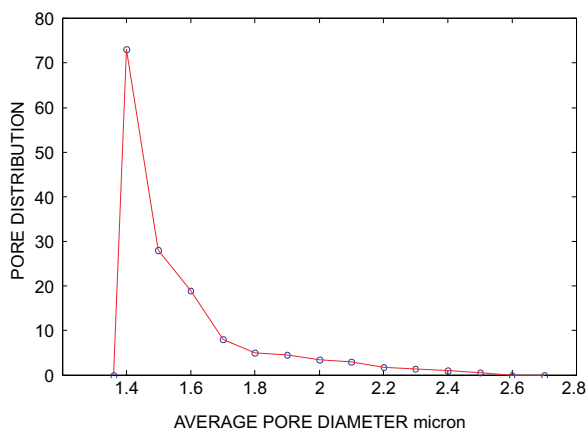


Figure 8. Pore distribution.

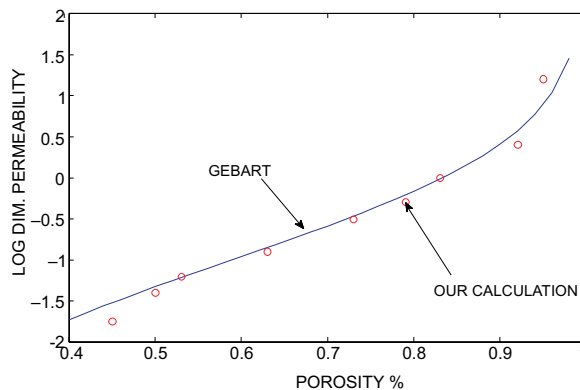


Figure 9. Permeability dependence on porosity.

The contour plots suggest that the lower concentration together with electric field increase gives lower fiber diameter. The stationary point is minimum values of the response or the smallest fiber diameter. The surface contour plots of these parameters outline the optimum condition for electrospinning (Figure 6).

Computational model for elastic property was matched with the experimental stress–strain curve for a PCL electrospun mesh. The tensile properties of electrospun fabrics were measured as a function of fiber diameter and density, and compared to those predicted using a mathematical model for fibrous networks. The resultant best fit for the effective Young’s modulus relative value was found to depend on fiber density and fiber diameter, which is shown in Figure 7.

By porosimetry method for electrospun fabric distribution pores related average pore diameters were determined (Figure 8). The distribution has the form of Gamma distribution (8).

Pore net model was determined for a given fiber (9). Using demo version of Pore-Cor software (10) the permeability of fibre net was determined as function of porosity (Figure 9). The calculated data were compared with permeability models for fibrous media (11) with acceptable error level.

## DISCUSSION

Experimental results and related mathematical models reveal that the elastic and transport properties of fibrous meshes are sensitive to the microstructural architecture. Processing parameters on one way influence process stability in one manner and microstructure space in the other. Future study will focus on the use of scaffolds in functional tissue engineering scenarios, with the application of tissue growth phenomena.

## REFERENCES

- METCALFE A D, FERGUSON M W J 2007 Bioengineering skin using mechanism of regeneration and repair. *Biomaterials* 28: 5100–5113

2. PORTER B, ZAUEL R, STOCKMAN H, GULDBERG R, FYHRIE D 2005 3-D computational modeling of media flow through scaffolds in a perfusion bioreactor. *J Biomechanics* 38: 543–549
3. HOLLISTERS S J, LIN C Y 2007 Computational design of tissue engineering scaffolds. *Comp. methods in app. mechanics and engineering* 196: 2991–2998
4. SENGERS B G, TAYLOR M, PLEASE C P, OREFFO R O C 2007 Computational modelling of cell spreading and tissue regeneration in porous scaffolds. *Biomaterials* 28: 1926–1940
5. ZIENKIEWICZ O 2005 *The Finite Element Method: Its basic and Fundamentals*, Elsevier, New York.
6. AGIC A 2008 Multiscale mechanical phenomena in electrospun carbon nanotube composites. *J Appl Polymer Science* 108: 1191–1200
7. MYERS R H, MONTGOMERY D C 1995 *Response surface methodology: process and product optimization using designed experiments*. Wiley-Interscience, New York.
8. EICHHORN S J, SAMPSON W W 2005 Statistical geometry of pores and statistics of porous nanofibrous assemblies. *J Royal Society Interface* 2: 309–318
9. GHASSEMZADEH J, SAHIMI M 2004 Pore network simulation of fluid imbibition into paper during coating: II. Characterization of paper's morphology and computation of its effective permeability tensor. *Chemical Engineering Science* 59: 2265–80
10. Pore-Cor Software, Environmental and Fluid Modelling Group, University of Plymouth, U.K.
11. GEBART B R 1992 Permeability of unidirectional reinforcements of RTM. *J Composite Mater* 26: 1100–33